



Preparation and characterization of WTiO₂ nanotubes decorated with Prussian blue nanoparticles and nanocubes with enhanced photoelectrochemical properties

Mohamad Mohsen Momeni¹ · Masoumeh Avazverdi¹

Received: 13 October 2020 / Revised: 25 March 2021 / Accepted: 31 March 2021 / Published online: 12 April 2021

© Australian Ceramic Society 2021

Abstract

Successive ionic layer adsorption and reaction (SILAR) method has been used to decorate Prussian blue (PB) on tungsten-doped titanium oxide nanotubes (WTiO₂). Scanning electron microscopy (SEM), X-ray diffraction (XRD), EDX, and UV-Vis-DRS methods have been used to characterize the morphology, phase composition, elemental composition, and optical properties of the samples prepared. The PB/WTiO₂ samples prepared were then used as photoanodes in photoelectrochemical water splitting to yield hydrogen. The morphology, optical property, and photoelectrochemical performance of the prepared samples were highly affected by the SILAR deposition cycle, according to the results obtained. The sample with PB deposited in 9 SILAR cycles (sample S9) showed the highest photocurrent value (0.118 mA/cm²) under illumination. This enhancement is mostly due to visible light harvesting and reduced recombination of photo-generated electron-hole pairs, resulting from the synergistic effect of the heterojunction and the well-organized morphology of WTiO₂.

Keywords SILAR · Prussian blue · Nanocubes nanotubes · Anodizing · Photoelectrochemical

Introduction

The efficient use of energy has become an important issue worldwide considering global warming [1]. The world is quickly turning into a global village due to the ever increasing need for energy to provide the increasing social and economic development, welfare, and health of humans. All societies require energy to meet their basic human needs including health, lighting, cooking, mobility, and communication. Two fundamental challenges of energy toward a sustainable future are the protection of energy supplies and restriction of energy contribution to climate changes. Surprisingly enough, over 1.4 billion of the world population do not have access to electricity while 85% of them live in the countryside [2]. Since it was first investigated by Fujishima, titanium dioxide (TiO₂) has become one of the best photocatalysts because of its extraordinary photoelectric, environmentally friendly, and stable

chemical properties [3, 4]. TiO₂ nanotubes can improve the visible light absorption and help the transfer of photoelectrons to the cathode in comparison with TiO₂ nanoparticles due to their unique geometry [5–7]. Compared with TiO₂ nanoparticles, the nanotube array structure both provides facile routes for electron transfer along the tubes to the electrical contact and allows the permeation of conductive electrolyte to the entire internal and external array surfaces. Hole transfer at the TiO₂/electrolyte interface can also be facilitated by TiO₂ nanotubes since the minority of carriers only need to diffuse across half thickness of the nanotube wall [7, 8]. Nevertheless, due to the wide band gap and easy recombination of photo-generated carries, TiO₂ nanotubes may only absorb in the UV region of solar energy and show limited photocatalytic performance [9]. To overcome these major obstacles, different modifications such as metal doping and non-metal doping, coupling with other semiconductors, noble metal deposition, quantum dot sensitization, and dye sensitizing, have been made [10–18].

The preparation of tungsten-doped titanium oxide nanotube (WTiO₂) arrays on titanium foil via one-step electrochemical anodization followed by deposition of Prussian blue (PB) on WTiO₂ by the successive ionic layer adsorption and reaction (SILAR) method from an aqueous ferric ferricyanide

✉ Mohamad Mohsen Momeni
mm.momeni@iut.ac.ir

¹ Department of Chemistry, Isfahan University of Technology, Isfahan 84156-83111, Iran

solution has been carried out. Prussian blue has been chosen due to its photostability and electrochemical activity. PB or iron (III) hexacyanoferrate (II) is well-known for its outstanding electrochemical, electrochromic, photophysical, and magnetic properties [19, 20]. The photoelectrochemical (PEC) properties of the photoelectrodes prepared were compared under illumination by xenon lamp.

Experimental section

Materials

Analytical grade chemicals were used without further purification prior to use. Distilled water (pH= 6.5, conductivity = 1.0–1.5 $\mu\text{S}\cdot\text{cm}^{-1}$) was used to prepare solutions. Titanium foils with purity and thickness of 99.9% and 1 mm, respectively, were purchased from Sigma-Aldrich.

Preparation of nanotubes photoanodes

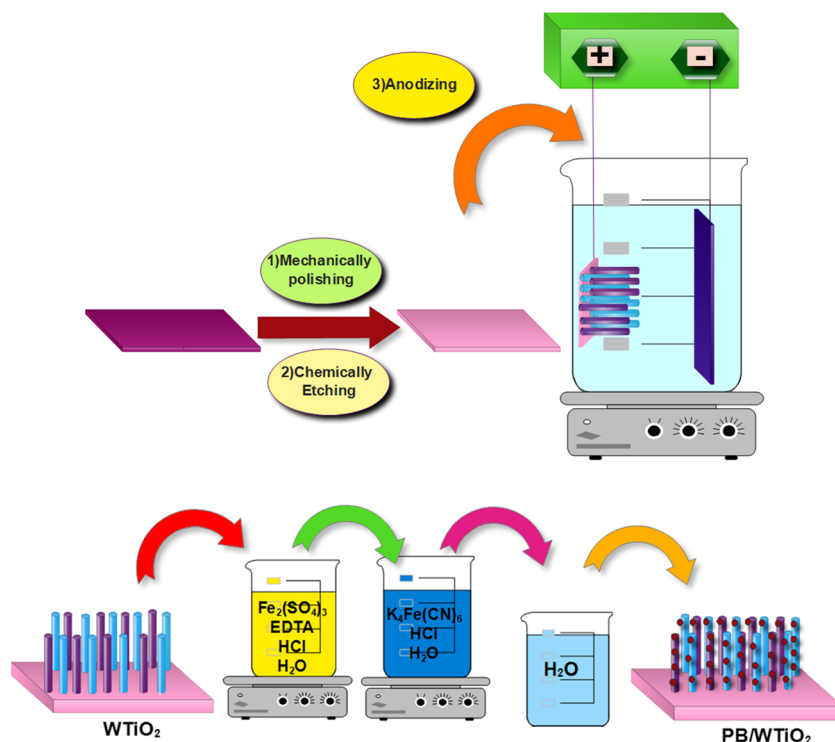
WTiO₂ nanotubes on titanium foil were prepared by electrochemical anodization of titanium in an appropriate electrolyte according to a method previously reported by this group [21, 22]. Having been anodized, the samples were annealed in oxygen atmosphere at 450°C for 2 h at a rate of 2°C/min to yield crystalline samples. Figure 1 shows the synthesis procedure for Prussian blue-sensitized WTiO₂ nanotube. Prussian

blue (PB) films were easily prepared through conventional SILAR method using two solutions. One of the solutions was prepared by mixing 15 ml of 0.1 mol/dm³ Fe₂(SO₄)₃, 90 ml of H₂O, 0.5 g of ethylenediaminetetraacetic acid (C₁₀H₁₆N₂O₈; EDTA), and 10 ml of 3 mol/dm³ HCl in a 250-ml beaker. The second solution was an aqueous solution containing 15 ml of 0.1 mol/dm³ K₄[Fe(CN)₆], 90 ml of H₂O, and 10 ml of 3 mol/dm³ HCl in a 250-ml beaker. The solutions were heated up to 50°C prior to deposition. The films were formed by successively immersing the substrates (WTiO₂/Ti) into the solutions between 2 and 3 seconds. The number of deposition cycles varied from 2 to 15 and the samples were labeled as S2, S3, S5, S7, S9, S10, and S15 accordingly. The number of deposition cycles was changed to optimize the amount of PB deposition on the WTiO₂ surface and the corresponding effect on the photoelectrochemical properties of the samples was investigated.

Sample characterization

Field emission scanning electron microscopy (Hitachi S-4160, Japan) was used to study the surface morphology of the samples prepared. The optical absorption properties of the annealed samples were characterized by UV-Vis spectroscopy (JASCO V-570) in the 300–600 nm range. The crystal structure of the samples was analyzed by X-ray diffraction analysis (XRD, Philips X'Pert PRO) using a Cu K radiation.

Fig. 1 Schemes of preparation of Prussian blue-sensitized WTiO₂ nanotubes via in situ anodizing and SILAR methods



Photoelectrochemical measurement

The PEC properties of the photoelectrodes were assessed using a 35-W xenon lamp illumination ($420 < \lambda < 700 \text{ nm}$) in 1.0-M potassium chloride (KCl) solution in a three-electrode photochemical quartz cell. A platinum foil and an Ag/AgCl (KCl saturated) were used as the counter and reference electrodes, respectively. The illuminated area of the prepared photoanode and the illumination intensity were 1 cm^2 and 100 mW/cm^2 , respectively.

Hydrogen production tests

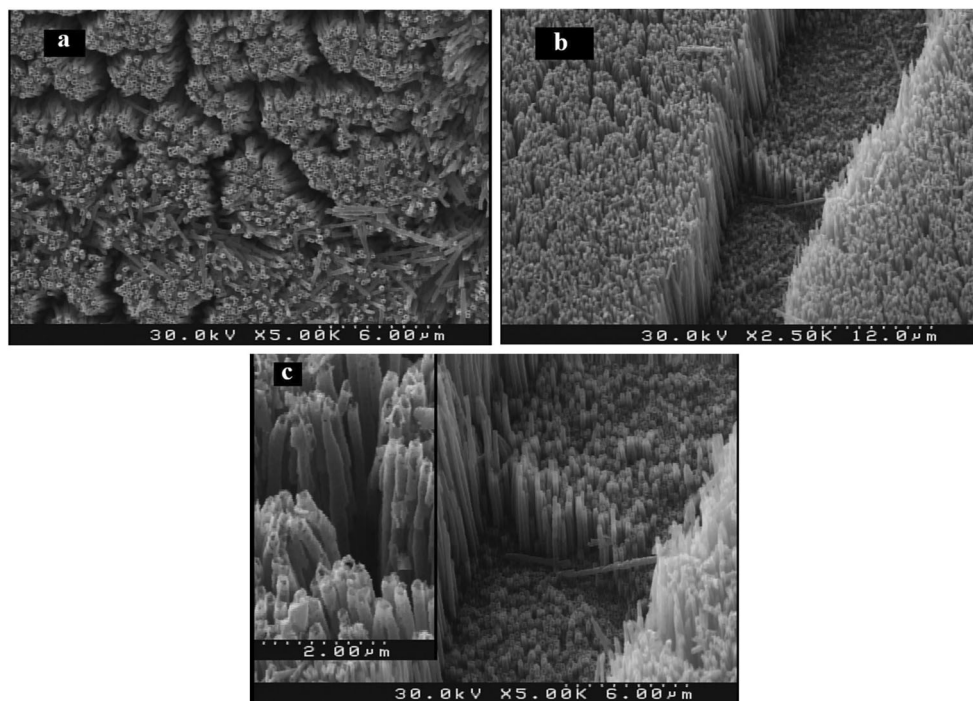
Hydrogen generation from the samples was recorded under a 35-W Xenon lamp illumination and H_2 gas was collected by water displacement technique based on a previously published procedure [6, 21, 22]. Hydrogen gas was formed at the counter electrode in the PEC cell.

Results and discussion

Field emission scanning electron microscopy (FE-SEM) was used to characterize the morphology of the prepared samples. Figure 2 shows micrographs of the as-synthesized WTiO_2 nanotubes grown on the titanium substrates. Nanotubes grew homogeneously over the substrate surface. The cross-section SEM image of WTiO_2 nanotubes layer shows that the obtained nanotubes are highly ordered and straight over their entire lengths. Figure 3 shows the FE-SEM images of different PB/

WTiO_2 nanotubes. The surface morphology of the WTiO_2 nanotube arrays prepared showed that the surface of the nanotubes was clean, without any cluster formation. The nanotubes prepared were open at the top end and closed at the bottom. Uniform nanotube arrays could be formed by the one-step anodization and the separated nanotubes may grow vertically on Ti substrates. The mechanism for the formation and surface properties of WTiO_2 nanotube arrays was extensively discussed in a previous work [22]. In addition, a tubular structure was shown by the FE-SEM images of PB/ WTiO_2 (Fig. 3a–g). Following the SILAR deposition, the smooth surface of the nanotube was covered by some nanoparticles and nanocubes, the size and amount of particles increasing as the number of SILAR cycles increased. At low immersion cycles, there was no evidence for the formation of nanocubes on the WTiO_2 nanotube surface. At high SILAR cycles, the formation of nanocubes on the nanotube surface can be clearly detected. As Fig. 3a and b shows, at low SILAR cycles, few nanocubes are scattered across the nanotube surface and the big size even blocks the tube opening. Careful observations show the dispersion of the nanoparticles on the surface without particle agglomeration. More nanocubes were formed on the tubes surface upon increasing the deposition cycle to 5. Further increase of the immersion cycle to 15 formed massive nanocubes with a 200- to 300-nm diameter range in some parts, which agglomerate and cover nearly the whole surface of WTiO_2 nanotube. As observed in Fig. 3g, the entire nanotube surface is covered by nanoparticles and nanocubes for fifteen SILAR cycles. According to the SEM results, the appropriate SILAR

Fig. 2 SEM images of the top surface and cross section of as-synthesized WTiO_2 nanotubes on Ti substrate with different magnifications



del "D:/Programs/ProductionJournal/Temp/coc.bat"

cycles favor uniform nucleation and growth of nanoparticles and nanocubes while very high SILAR cycles lead to the particle agglomeration.

Figure 4 shows the XRD patterns of the PB/WTiO₂ sample synthesized in which Prussian blue was prepared by 9 SILAR cycles. The coatings mostly consist of TiO₂, confirming the

crystalline nature of the nanotubes and the presence of anatase phase (JCPDS card No. 00-021-1272), as one would expect for titanium nanotubes annealed at 450°C. Two characteristic peaks are observed at $2\theta = 17.6^\circ$ (200) and 35.4° (400), which match the standard pattern of Prussian blue (JCPDS 01-073-0687). It can be said that due to the dispersion and incorporation of tungsten in the crystal lattice of TiO₂, no characteristic peak attributed to tungsten oxide can be found in this XRD

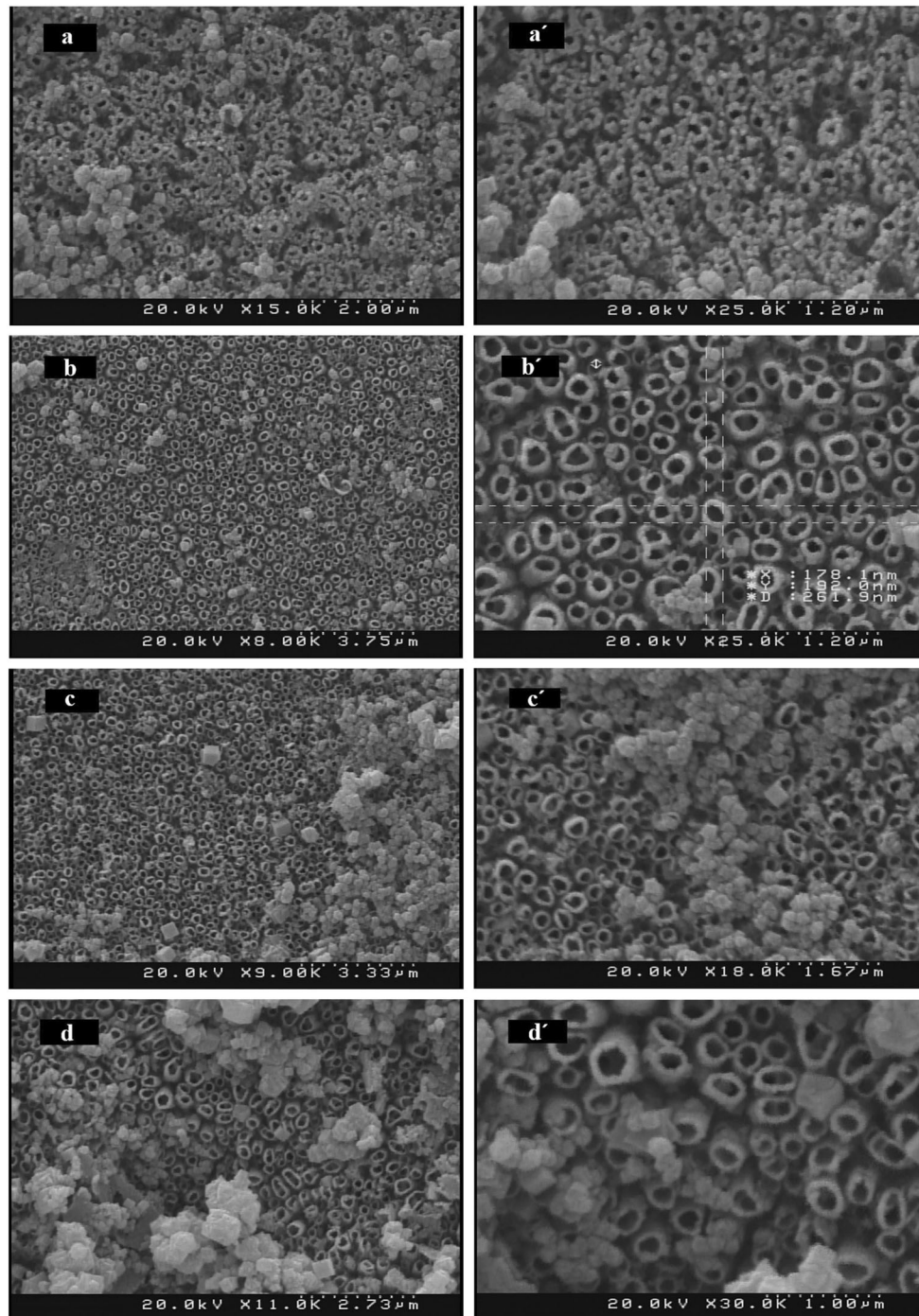


Fig. 3 SEM top-view images of prepared samples with different magnifications: **a** sample S2, **b** sample S3, **c** sample S5, **d** sample S7, **e** sample S9, **f** sample S10, and **g** sample S15

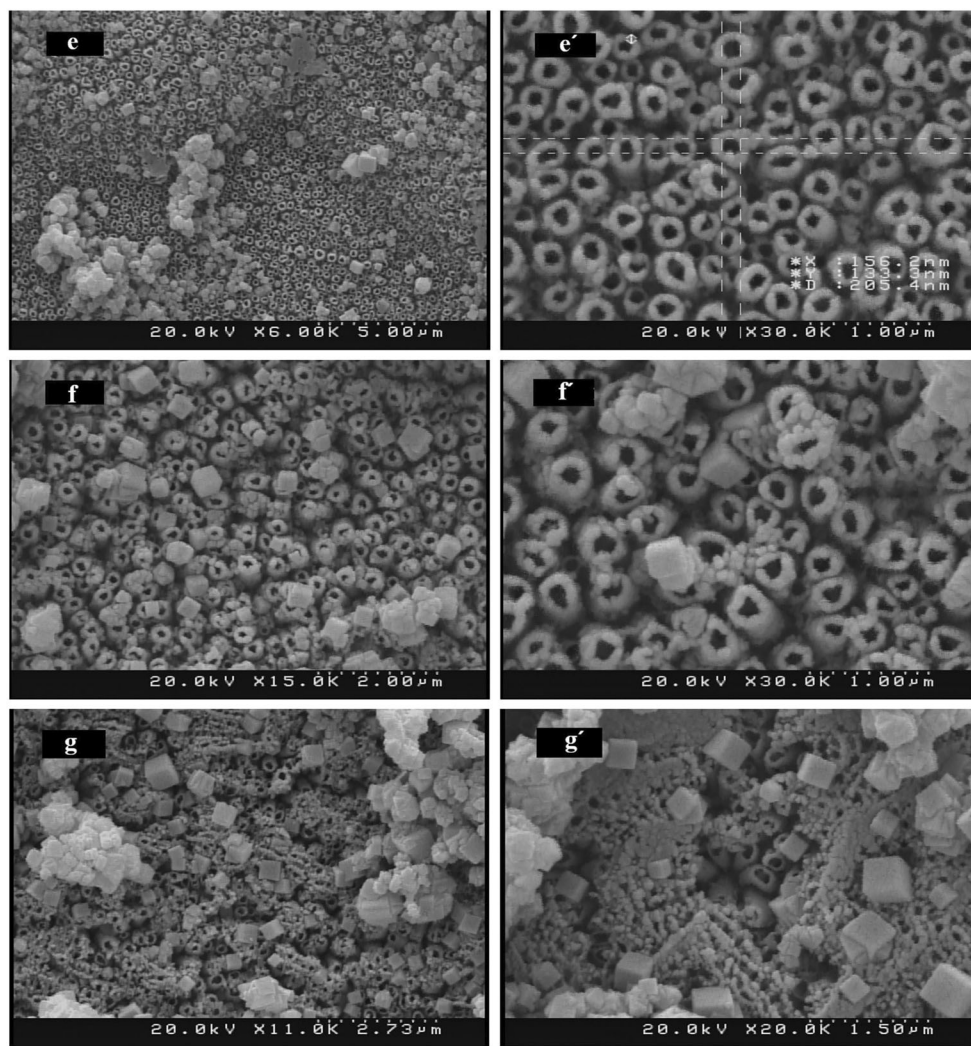


Fig. 3 (continued)

pattern. Energy dispersive X-ray spectroscopy (EDX) was used to analyze the chemical composition of the electrodes obtained. The elemental EDX images of pure WTiO₂ and

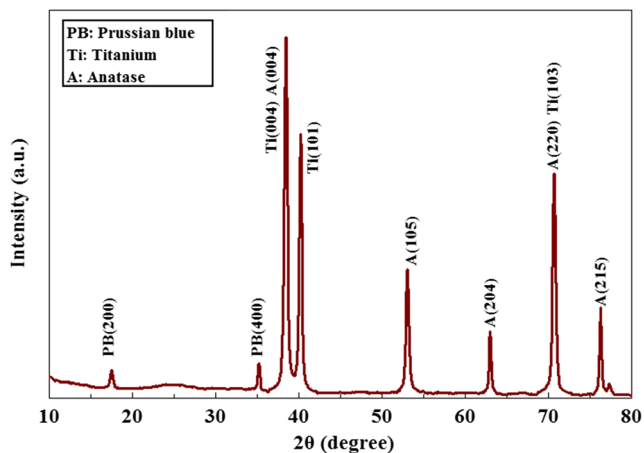


Fig. 4 XRD pattern of sample S9 annealed at 400°C

PB/WTiO₂ electrodes prepared by SILAR method are shown in Figs. 5 and 6, respectively. Energy dispersive X-ray spectroscopy (EDS) is an analytical process that identifies the elements (and their composition) present in prepared samples. As observed in Fig. 5, the characteristic peaks in the spectrum of uncoated WTiO₂ nanotubes are due to Ti, O, and W. Three new peaks are observed in the EDX images of PB/WTiO₂ electrodes, which are associated with Fe, C, and N in addition to the peaks ascribed to pure WTiO₂ nanotubes (Fig. 6).

The UV-Vis diffuse reflectance absorption spectra (DRS) of the uncoated WTiO₂ and different PB/WTiO₂ electrodes in the 300–600 nm range are shown in Fig. 7. UV-Vis most often refers to absorption spectroscopy, measured by transmission, whereas DRS specifically refers to diffuse reflection spectroscopy. Normally, the former is used for solutions/suspensions, whereas the latter is used for films or powders. The strong absorption observed in a wavelength below 400 nm corresponds to the intrinsic interband transition absorption of TiO₂-based semiconductors. Very low absorptions are

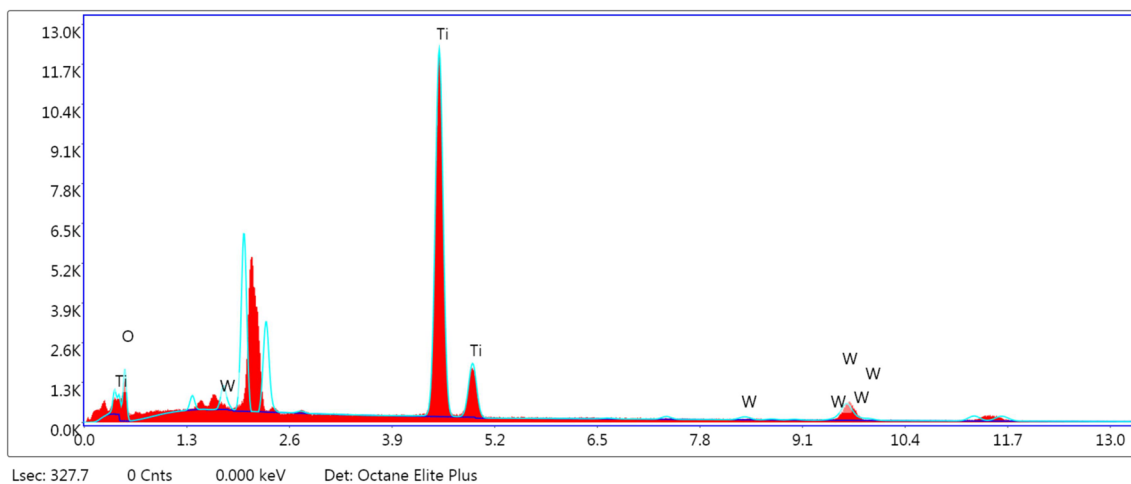


Fig. 5 EDX spectrum of uncoated WTiO₂ nanotubes

observed in the UV-Vis spectrum of pure WTiO₂ in the visible light region. However, PB/WTiO₂ electrodes exhibit higher absorptions in the visible light. In addition, increasing the amount of Prussian blue on the film has increased visible light absorption. The redshifts observed upon increasing the amount of Prussian blue of the sample films show that the band gap energy of the samples has slowly decreased. On the other hand, the light absorption range is broadened by the PB particle deposition. Therefore, increasing the number of SILAR cycles increases the absorption edge of the spectra redshift and the absorbance in the visible range. A Tauc plot can be created by a Kubelka-Munk transformation on the UV-Vis absorption data to estimate the band gap energy of the electrodes prepared with various SILAR cycle numbers [23–26]. The Kubelka-Munk function, $[F(R_{\infty})/hv]^{1/2}$, is determined by $(ahv)^{1/2}$, in which hv and a are the photon energy and the absorption coefficient, respectively [26]. Plotting $(ahv)^{1/2}$ vs. hv gives a Tauc plot. Consequently, the approximate optical band gap energies measured were 2.80, 2.72, 2.70, 2.60, 2.58, 2.66, and 2.40 eV for the S2, S3, S5, S7,

S9, S10, and S15 samples, respectively. As observed, band gap values decrease upon increasing the deposition process cycles (n) from 2.90 eV for uncoated WTiO₂ to 2.40 eV after 15 immersion cycles ($n = 15$). The minimum band gap energy is shown by sample S15 since it has the highest Prussian blue amount. The electron-hole pairs can be excited by lower energy visible light to participate in the photocatalytic process due to band gap narrowing. The photoelectrochemical activity of WTiO₂ should be enhanced by loading with Prussian blue due to the intensification and effective broadening of the absorption to the visible region.

Amperometric measurements under intermittent illumination were used to study the photocurrent response of the samples prepared. I-t curves obtained from the PEC cell PB/WTiO₂ (apparent surface area of 1×1 cm²) and a platinum foil (apparent surface area of 2×2 cm²) as the anode and cathode, respectively, at 0.6 V vs. Ag/AgCl are shown in Fig. 8. As observed in this figure, regular ups and downs are shown by the PB/WTiO₂ photoelectrodes along light on and off. The current increases immediately and reaches a steady state for

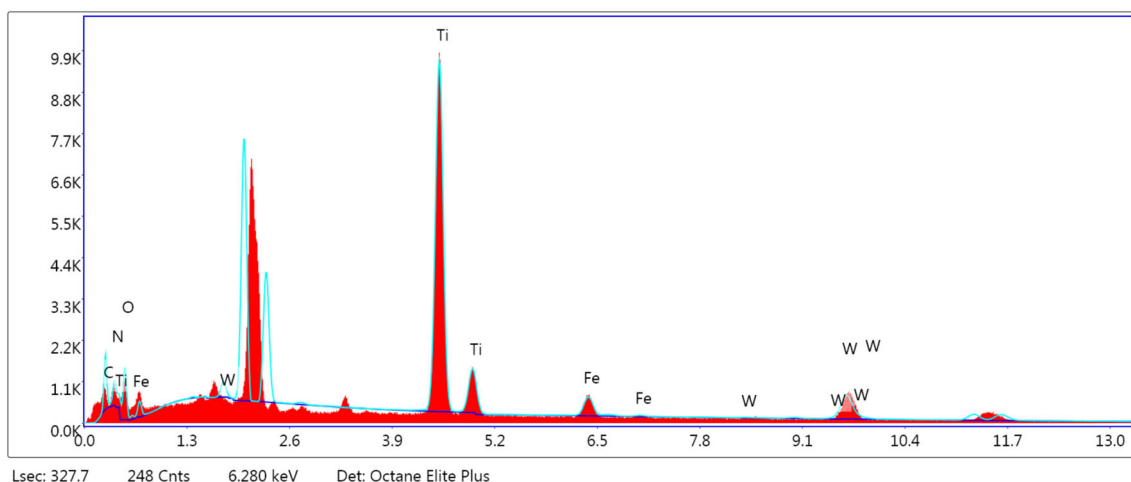


Fig. 6 EDX spectrum of sample S9

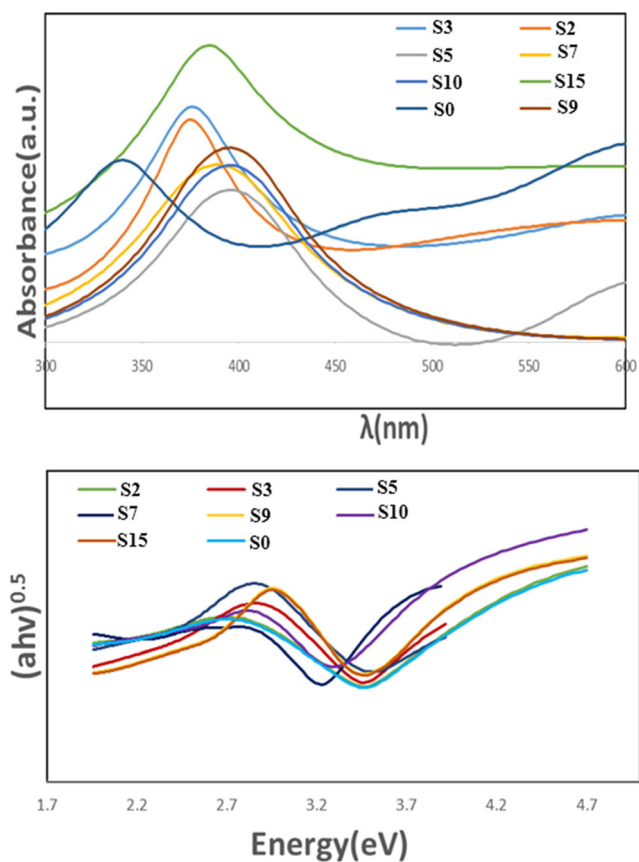
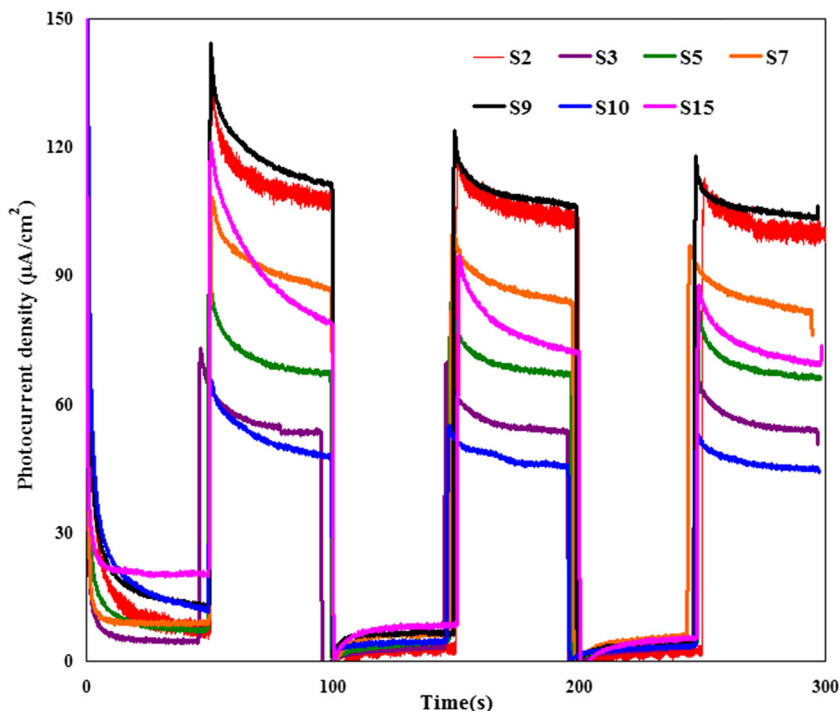


Fig. 7 UV-Vis absorption spectra and direct band gap of prepared samples

each sample upon beginning of illumination. The data indicates a very low dark current for all samples prepared. The

Fig. 8 I_{ph} -t curves (on-off cycles) of samples at an applied potential of 0.6 V vs. Ag/AgCl



photocurrent densities are highly affected by the SILAR deposition. Sample S9 (SILAR cycle=9) shows the highest photocurrent value. In addition, the photocurrent density of 0.118 mA/cm² is 1.05-, 2.14-, 1.68-, 1.3-, 2.41-, and 1.44-folds of the corresponding values for S2, S3, S5, S7, S10, and S15, respectively. Similar results are observed in the J-V curves. Moreover, S9 photoelectrode shows the optimal photoelectric efficiency along the increased applied bias. The presence of a regular structure of nanotubes on the surface of sample S9 increases the surface area. The increasing surface area would improve the light absorption which consequently could increase the photocurrent density of this sample. In sample S15, most of the nanotubes are covered by nanoparticles and nanocubes, which reduces its active surface area and its ability to absorb light is reduced; therefore, it shows weak photoelectric efficiency. PB/WTiO₂ nanotubes with different cycles of deposition of PB also show photoanodic behavior.

Figure 9 shows the photovoltages of PB/WTiO₂ electrodes investigated by OCP. The OCP response was used to evaluate the electrons resulting from band gap excitation of PB/WTiO₂ photoelectrodes and accumulated at the electrode surface under light irradiation and open-circuit conditions. Upon switching the light on, the OCPs of these photoanodes negatively shift due to the generation of photo-induced electrons and their accumulation on the electrode surface. The OCPs of these photoanodes positively shift immediately upon switching the light off. Surface photovoltage is quickly produced by these new photoelectrodes when the Xe lamp is switched on and the values remain stable during light irradiation. S9 photoelectrode produces the highest photovoltage

Fig. 9 Photo-induced potential-time response (OCP-time) curves of photoelectrodes

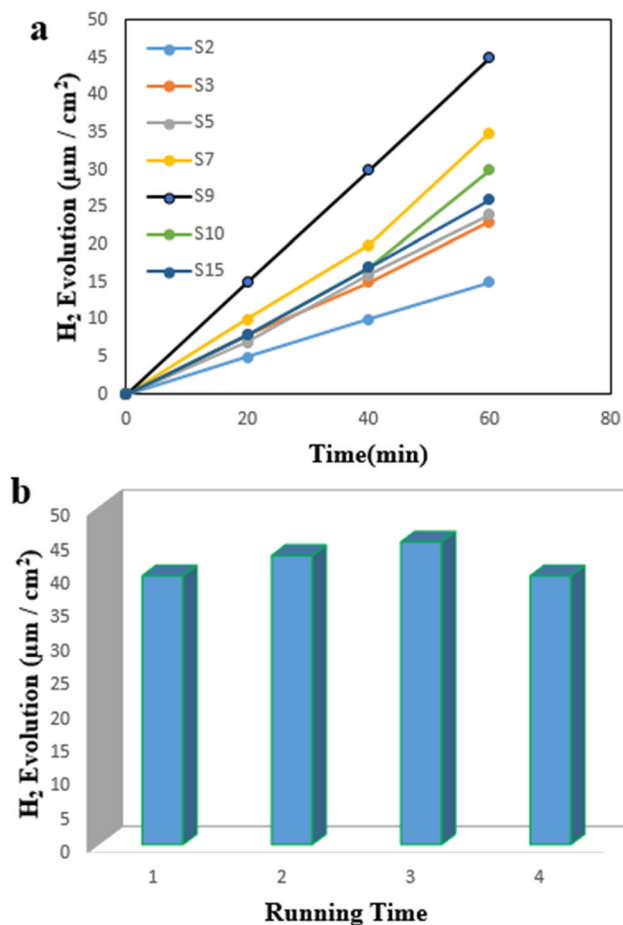
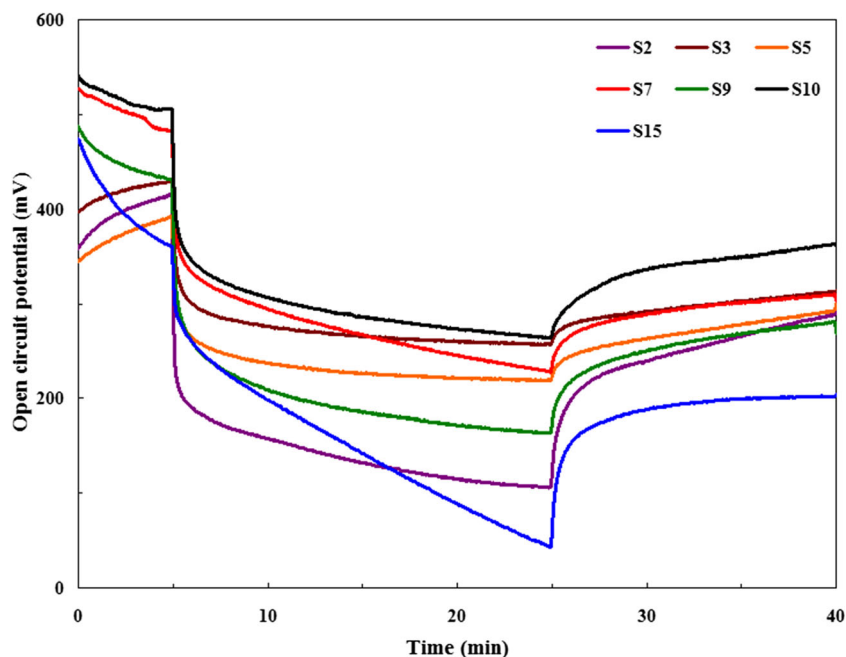


Fig. 10 Comparison of the hydrogen evolution rate for different photoelectrodes and stability test of hydrogen production for sample S9

(0.12 V/cm²). Maximum photo-induced potential drop of approximately 300 mV is shown by S9 photoanode, which confirms that the PEC conversion performance under light illumination has been considerably improved by the Prussian blue.

Hydrogen evolution measurement in a three-electrode system was used to evaluate the PEC water splitting performance of various photoanodes [22, 27]. The working electrode was set at a bias potential of +0.6 V vs. Ag/AgCl and illumination was provided by a 100 mW cm⁻² xenon lamp light during the gas evolution process. The hydrogen generation rates in 1 h for samples S2, S3, S5, S7, S9, S10, and S15 are 15, 23, 24, 35, 45, 30, and 26 μl/cm², respectively (Fig. 10a). The hydrogen generation rate by sample S9 is clearly the highest, as expected from the photocurrent density values. Since photocatalyst recyclability is a major concern with regard to practical applications, so hydrogen productions of sample S9 as a function of sequence of reaction time under the conditions described in this work were studied, and the result is shown in Fig. 10b. Hydrogen production rate has no obvious decay and maintains an average value of 45 μl/cm² after four continuous cycles, indicating the good chemical stability of the composites synthesized by this method in photoelectrochemical process and their potential for long-term hydrogen production.

Conclusion

Prussian blue/WTiO₂ nanotube (PB/WTiO₂) nanocomposite has been prepared through titanium anodization and SILAR

method. The surface morphology, phase composition, structural, and optical properties of PB/WTiO₂ samples sensitized have been studied. According to the results, the morphology, visible light response, and photoelectrochemical properties were considerably affected by the SILAR deposition cycle, and promising harvesting and optimal photocurrent under xenon light irradiation were shown by sample S9 prepared with 9 SILAR cycles. The photovoltage and photocurrent density of sample S9 photoelectrode were 0.12 V/cm² and 0.118 mA/cm², respectively. The improved photocatalytic properties can be due to the extended absorption in the visible light region and efficient separation of photo-generated electron-hole pairs by Prussian blue deposition on the WTiO₂ nanotube.

References

- Owusu, P.A., Asumadu-Sarkodie, S.: A review of renewable energy sources, sustainability issues and climate change mitigation. *Cogent Eng.* **3**, 1167990 (2016)
- Momeni, M.M., Hakimian, M., Kazempour, A.: Preparation and characterisation of manganese-TiO₂ nanocomposites for solar water splitting. *Surf. Eng.* **32**, 514–519 (2016)
- Fujishima, A., Honda, K.: Electrochemical Photolysis of Water at a Semiconductor Electrode. *Nature.* **238**, 37–38 (1972)
- Fujishima, A., Rao, T., Tryk, D.: Titanium dioxide photocatalysis. *J. Photochem. Photobiol. C.* **1**, 1–21 (2000)
- Dong, Z., Ding, D., Li, T., Ning, C.: Facile fabrication of Si-doped TiO₂ nanotubes photoanode for enhanced photoelectrochemical hydrogen generation. *Appl. Surf. Sci.* **436**, 125–133 (2018)
- Momeni, M.M., Ghayeb, Y.: Photoinduced deposition of gold nanoparticles on TiO₂-WO₃ nanotube films as efficient photoanodes for solar water splitting. *Appl. Phys. A Mater. Sci. Process.* **122**, 620 (2016)
- Li, Y., Cao, C., Xie, X., Zhang, L., Lin, S.: Enhanced photoelectrochemical performance of TiO₂ nanotube arrays with coexisted Pt nanoparticles and Co-Pi cocatalysts. *Appl. Surf. Sci.* **436**, 337–344 (2018)
- Zeng, M., Peng, X.E., Liao, J.J., Wang, G.Z., Li, Y.F., Li, J.B., Qin, Y., Wilson, J., Song, A.M., Lin, S.W.: Enhanced photoelectrochemical performance of quantum dot-sensitized TiO₂ nanotube arrays with Al₂O₃ overcoating by atomic layer deposition. *Phys. Chem. Chem. Phys.* **18**, 17404–17413 (2016)
- Wang, J.W., Xu, G.Q., Zhang, X., Zhai, P.B., Lv, J., Wang, D.M., Zheng, Z.X., Wu, Y.C.: Photoelectrochemical performances of TiO₂ nanotube arrays hydrothermally treated in sulfide. *Appl. Surf. Sci.* **363**, 644–650 (2016)
- Zhang, L., Pan, N.Q., Lin, S.W.: Influence of Pt deposition on water-splitting hydrogen generation by highly-ordered TiO₂ nanotube arrays. *Int. J. Hydrog. Energy.* **25**, 13474–13480 (2014)
- Yang, L., Zhang, M., Zhu, K.R., Lv, J.G., He, G., Sun, Z.Q.: Electrodeposition of flake-like Cu₂O on vertically aligned two-dimensional TiO₂ nanosheet array films for enhanced photoelectrochemical properties. *Appl. Surf. Sci.* **391**, 353–359 (2017)
- Park, J.H., Kim, S.W., Bard, A.J.: Novel carbon-doped TiO₂ nanotube arrays with high aspect ratios for efficient solar water splitting. *Nano Lett.* **6**, 24–28 (2005)
- Ye, M.D., Gong, J.J., Lai, Y.K., Lin, C.J., Lin, Z.Q.: High-efficiency photoelectrocatalytic hydrogen generation enabled by palladium quantum dots-sensitized TiO₂ nanotube arrays. *J. Am. Chem. Soc.* **134**, 15720–15723 (2012)
- Momeni, M.M., Ghayeb, Y., Mozafari, A.A.: Optical and photo catalytic characteristics of Ag₂S/TiO₂ nanocomposite films prepared by electrochemical anodizing and SILAR approach. *J. Mater. Sci. Mater. Electron.* **27**, 11201–11210 (2016)
- Hu, S.J., Wang, B.L., Zhu, M.S., Ma, Y.H., Lv, Z.H., Wang, H.: High-performance 1D type-II TiO₂@ZnO core-shell nanorods arrays photoanodes for photoelectrochemical solar fuel production. *Appl. Surf. Sci.* **403**, 126–132 (2017)
- Peng, C.C., Wang, W.Z., Zhang, W.W., Liang, Y.J., Zhuo, L.: Surface plasmon driven photoelectrochemical water splitting of TiO₂ nanowires decorated with Ag nanoparticles under visible light illumination. *Appl. Surf. Sci.* **420**, 286–295 (2017)
- Zhu, W., Liu, X., Lin, H.Q., Tong, D.L., Yang, J.Y., Peng, J.Y.: Coaxial heterogeneous structure of TiO₂ nanotube arrays with CdS as a super thin coating synthesized via modified electrochemical atomic layer deposition. *J. Am. Chem. Soc.* **132**, 12619–12626 (2010)
- Subramanian, A., Pan, Z.H., Li, H.F., Zhou, L.S., Li, W.F., Qiu, Y.C., Xu, Y.J., Hou, Y., Muzi, C., Zhang, Y.G.: Synergistic promotion of photoelectrochemical water splitting efficiency of TiO₂ nanorods using metal-semiconducting nanoparticles. *Appl. Surf. Sci.* **420**, 631–637 (2017)
- Pyrasch, M., Toutianoush, A., Jin, W., Schnepf, J., Tiede, B.: Self-assembled Films of Prussian Blue and Analogues: Optical and Electrochemical Properties and Application as Ion-Sieving Membranes. *Chem. Mater.* **15**, 245–254 (2003)
- Itaya, K., Uchida, I., Neff, V.D.: Electrochemistry of polynuclear transition metal cyanides: Prussian blue and its analogues. *Acc. Chem. Res.* **19**, 162–168 (1986)
- Momeni, M.M., Ghayeb, Y., Shafei, M.: Preparation and characterization of CrFeWTiO₂ photoanodes and their photoelectrochemical activities for water splitting. *Dalton Trans.* **46**, 12527–12536 (2017)
- Momeni, M.M., Ghayeb, Y., Davarzadeh, M.: Single-step electrochemical anodization for synthesis of hierarchical WO₃-TiO₂ nanotube arrays on titanium foil as a good photoanode for water splitting with visible light. *J. Electroanal. Chem.* **739**, 149–155 (2015)
- Mollavali, M., Falamaki, C., Rohani, S.: High performance NiS-nanoparticles sensitized TiO₂ nanotube arrays for water reduction. *Int. J. Hydrog. Energy.* **41**, 5887–5901 (2016)
- Lui, G., Liao, J.Y., Duan, A., Zhang, Z., Fowler, M., Yu, A.: Graphene wrapped hierarchical TiO₂ nanoflower composites with enhanced photocatalytic performance. *J. Mater. Chem. A.* **1**, 12255–12262 (2013)
- Sakthivel, S., Janczarek, M., Kisch, H.: Visible light activity and photoelectrochemical properties of nitrogen-doped TiO₂. *J. Phys. Chem. B.* **108**, 19384–19387 (2004)
- Li, Y., Wei, L., Chen, X., Zhang, R., Sui, X., Chen, Y.: Efficient PbS/CdS co-sensitized solar cells based on TiO₂ nanorod arrays. *Nanoscale Res. Lett.* **8**, 1–7 (2013)
- Momeni, M.M., Ghayeb, Y., Ezati, F.: Fabrication, characterization and photoelectrochemical activity of tungsten-copper co-sensitized TiO₂ nanotube composite photoanodes. *J. Colloid Interface Sci.* **514**, 70–82 (2018)

Publisher's note Springer Nature remains neutral with regard to jurisdictional claims in published maps and institutional affiliations.